# On the effectiveness of ventilation to mitigate the damage of spherical chambers subjected to confined trinitrotoluene detonations

**Article** · September 2018

CITATIONS
0

READS
81

**3 authors**, including:

Francisco Hernandez
University of Chile
**31** PUBLICATIONS **42** CITATIONS
SEE PROFILE

Xihong Zhang
Curtin University
**42** PUBLICATIONS **443** CITATIONS
SEE PROFILE

*Research Paper*

Advances in Structural Engineering

Advances in Structural Engineering
1–16

DOI: 10.1177/1369433218791610
journals.sagepub.com/home/ase
SAGE

# On the effectiveness of ventilation to mitigate the damage of spherical chambers subjected to confined trinitrotoluene detonations

**Francisco Hernandez[1], Hong Hao[2] and Xihong Zhang[2]**

## Abstract

This article presents a comparative study on the effectiveness of ventilation to mitigate blasting effects on chambers subjected to confined detonations of high explosives. The pressure time-history that acts on the chamber walls is described by three components: (1) the first shock wave, (2) the train of re-reflected shock waves, and (3) the gas pressure. The radial response of spherical chambers is described by the radial breathing mode and modeled by an equivalent single degree of freedom system. The three pressure components are considered for the calculation of the maximum ductility ratio, which is obtained from the numerical solution of the single degree of freedom chamber response. It is assumed that openings reduce the gas pressure but they have an insignificant effect on shock waves. The dynamic response of fully and partially confined chambers are calculated and compared. Results show that intermediate/small openings (less than 10% of the surface of the chamber) are ineffective to mitigate the chamber response and damage. The vibratory response of the chamber is susceptible to elastic or plastic resonance but it is not considerably modified by the long-term gas pressure because of its high radial breathing mode frequency, allowing concluding that ventilation is ineffective to reduce the maximum response of spherical chambers subjected to internal high explosive explosion.

## Keywords

afterburning, fully and partially confined explosions, gas pressure component, high explosive, plastic resonance, ventilation

## Introduction

A blast chamber is a structural system designed to confine internal explosions to prevent casualties and damage of surrounding facilities and structures. A blast chamber can be designed for single or multiple usages. A multiple-usage chamber is designed to remain elastic under the action of blasting loads, while single-usage chambers can undergo a controlled level of damage.

The first analytical solution of explosion containment chambers was published in 1950s by Baker and Allen (1958). In that study, the elastic response of spherical chambers, which are subjected to a uniformly distributed internal transient pressure, was obtained using an equivalent single degree of freedom (SDoF) system and then expanded to consider its elastic–plastic response (Baker, 1960). White and colleagues (White et al., 1977, White and Trott, 1980) concluded that an increment in the static yield strength of the tank material can improve the agreement between the analytical and experimental results.

It is commonly agreed that openings and frangible covers can be useful to reduce the structural damage of blast chambers and provide more effective designs, based on the fact that ventilation should reduce the pressure intensity associated with an internal explosion (Eckhoff, 2013). In fact, the pressure time-history is highly susceptible to ventilation when a confined deflagration occurs (Bradley and Mitcheson, 1978; BS EN 14494:2007, 2007; Chippett, 1984; Hernandez et al., 2015; Molkov et al., 2000, 2004; NFPA 68, 2007; Puttock et al., 2000; Yao et al., 1969).

In contrast, a high explosive (HE) generates a detonation that is characterized by a supersonic combustion that triggers a train of shock waves. In fact, the pressure time-history, which acts on chamber walls subjected to fully or partially confined HE detonations, is commonly described by three components. In this context, the three pressure components that are

[1]Department of Civil Engineering, University of Chile, Santiago, Chile
[2]Department of Civil Engineering, Curtin University, Perth, WA, Australia

**Corresponding author:**
Francisco Hernandez, Department of Civil Engineering, University of Chile, Av. Blanco Encalada 2002, Santiago 8370449, Chile.
Email: fhernandezp@ing.uchile.cl

generated by confined HE detonations that occur on spherical chambers have been described from theoretical derivations (Abakumov et al., 1984; Belov et al., 1986; Zhdan, 1981), numerical simulations (Donahue et al., 2013; Dong et al., 2012; Hernandez et al., 2016; Li et al., 2008), and observed from experimental data (Adishchev and Kornev, 1979; Anderson et al., 1983; Belov et al., 1986; Beshara, 1994; Buzukov, 1980; Chan and Klein, 1994; Donahue et al., 2013; Dong et al., 2012; Hernandez et al., 2016; Karpp et al., 1983; Li et al., 2008). The first component is an impulsive component caused by the reflection of the first shock wave, which propagates supersonically from the detonation point until it reaches the chamber wall. The second component is a train of re-reflected shock waves, caused by consecutive reflections of the first shock wave on the chamber walls; this train of shock waves is successively attenuated due to its interaction with air, which transforms the kinetic energy allocated into the shock waves to internal energy through a viscous dissipation process. Finally, the quasi-static gas pressure component is generated because the kinetic energy allocated into the shock waves is slowly transformed to internal energy, causing that the enclosed gases (HE products and air) increase their temperature and pressure if they are restrained to expand freely.

Even though it is conventionally accepted that ventilation reduces the gas pressure and impulse, there is a lack of detailed studies of shock wave propagation and gas pressure interaction of containment structures with openings or frangible covers. In fact, there is not a clear understanding about the effectiveness that openings and vents can provide when an internal HE detonation occurs.

The pressure time-history can be approximately estimated when symmetrical chambers, such as spherical or cylindrical geometries, are subjected to concentric trinitrotoluene (TNT) detonations. That is, the three pressure components (the first shock wave, the train of re-reflected shock waves, and the gas pressure) can be estimated using simplified approaches (Baker and Kulesz, 1983; UFC 3-340-02, 2008). Based on these simplified pressure components, the linear and nonlinear response of spherical chambers subjected to concentric internal explosion can be calculated based on an equivalent SDoF system. As a result, the influence of each pressure component on the peak response can be analyzed to understand their effects. Particularly, the effect of the reduction of the gas pressure component due to ventilation can be analyzed to explain how it mitigates damage of spherical chambers.

In this study, the analysis is focused on realistic idealized scenarios of spherical monobloc steel vessels subjected to detonation of concentric spherical TNT charges. Multiple numerical analyses are performed that allow covering a wide range of parameters: diameter of chamber (0.5–6 m), equivalent TNT charge weight (0.05–400 kg), and ductility ratios (0.2–8.0). All results are summarized in terms of a dimensionless thickness, which allows comparing different chamber scales and charge weight densities. Conclusions about the consequence of each pressure component are then analyzed. Results indicate that ventilation is not necessarily an effective technology to reduce damage related to the vibratory response of storage chambers subjected to an internal HE detonation.

## Simplified analysis: equivalent SDoF system

The dynamic response of monobloc thin walls spherical chambers that are subjected to uniformly distributed pressure time-histories ($p(t)$) can be described by an equivalent SDoF system related to its radial breathing mode (RBM) (Baker, 1960). Based on these derivations, the equation of motion that describes the elastic RBM displacement is expressed as follows ($u_r$)

$$\frac{\partial^2 u_r}{\partial t^2} + {\omega_n}^2 \cdot u_r = \frac{p(t)}{\rho \cdot h} \tag{1}$$

where the parameters that describe the perfect elastic–plastic SDoF system are: the equivalent mass ($m = \rho \cdot h$), the equivalent elastic stiffness ($k = 2 \cdot h \cdot E/(1-\nu) \cdot a^2$), the natural angular frequency ($\omega_n = \sqrt{2 \cdot E/\rho(1-\nu) \cdot a^2}$), and the equivalent yielding pressure ($P_y = 2 \cdot h \cdot \sigma_y/a$); where $\rho$ is the material density (kg/m$^3$), $h$ is the chamber wall thickness (m), $\nu$ is the material Poisson's ratio, $E$ is the material Young's modulus (Pa), $\sigma_y$ is the yielding strength (Pa), $t$ is the time, and $a$ is the mean radius of the chamber (mm) (Baker, 1960).

Without losing generalization of found results, the chamber material assumed during this study is steel BHW35, that is, the same material that was analyzed by Dong et al. (2012) for a spherical blast chamber that was tested subjected to a 25 kg of a concentric charge of TNT. That is, the elastic properties are the commonly employed for steel, that is, $E = 2.17 \times 10^5$ MPa, $\rho = 7.8 \times 10^3$ kg/m$^3$, and $\nu = 0.28$. The yield strength for steel BHW35 (high-strength steel) is $\sigma_y = 390$ MPa. Strain-rate effects are ignored because results are presented in terms of a dimensionless thickness, which is independent of the selected material properties.

During the initial studies of spherical chambers subjected to concentric HE detonations, the pressure time-history was idealized by an unique equivalent triangular pulse (Baker, 1960; Baker and Allen, 1958).

**Table 1.** Comparative blasting scenarios.

| Case | Description | Sketch |
|---|---|---|
| 1S | The pressure time-history is modeled using a triangular pulse associated with the first shock wave only (obtained from UFC's charts). | 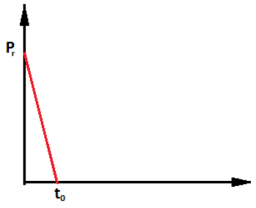 |
| 1S + QSG | The pressure time-history is obtained using the envelope between the first reflected shock wave (estimated from UFC charts) and a constant QS gas pressure function (which is also obtained from the UFC's charts). This case models simplistically the fully confined case. | 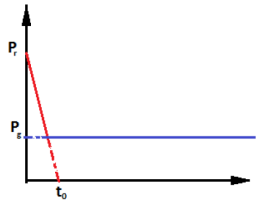 |
| 1S + TG | The pressure time-history is estimated using the maximum between the triangular pulse associated with the first shock wave (estimated from UFC charts) and the gas pressure component according to a triangular function based on UFC's approach. This case corresponds to the partially confined case defined by the UFC. A vent area equal to 25% of the chamber's surface has been considered for this case. | 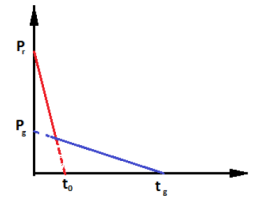 |
| 3S | The pressure time-history is modeled using a triangular pulse associated with the reflected first shock wave (estimated from UFC charts) and two subsequent reflected shock waves according to Baker's approach (three re-reflected shock waves with decaying amplitudes). | 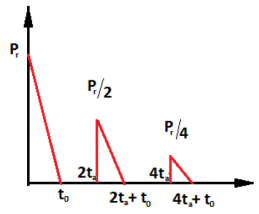 |
| 3S + QSG | The pressure time-history is obtained using the superposition of the three re-reflected shock waves of Case 3S and the gas pressure component estimated from UFC's charts. This case corresponds to the fully confined case. The gas pressure component grows linearly until it reaches the QS gas pressure at the end of the third shock wave. | 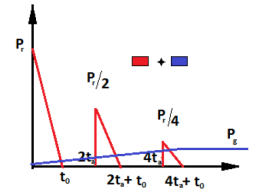 |
| 3S + TG | The pressure time-history is obtained using the superposition of the three reflected shock (3S) and the gas pressure component associated with the partially confined case (estimated from UFC's charts) and assuming a vent area equivalent to 10% of the chamber's surface. | 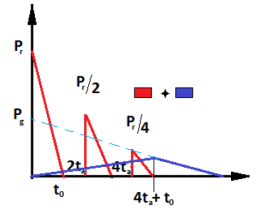 |

However, the simplified blast pressure ($p(t)$) can be better described by including the three pressure components, which can be taken into account when the chamber response is solved using numerical integration methods. Moreover, the response associated with each pressure component can be analyzed separately (or simultaneously) in order to understand its effect on the chamber response. Based on this, the software

MATLAB 7.9.0 will be employed to (1) digitalize and estimate the blast loading components from simplified blast loading approaches, (2) obtain the numerical non-linear response of the equivalent SDoF system (Newmark's constant acceleration method (Chopra, 1995)), and (3) compare the effect of each pressure component and the ventilation on the chamber response related to the blast scenarios (Table 1).

## Simplified energy approach to determine the chamber thickness

Based on the equivalent perfect elastic–plastic SDoF system, the ductility ratio ($\mu$) is defined as the ratio between the peak radial displacement and the yielding radial displacement ($\mu = u_{r-\max}/u_{ry}$, where $u_{ry} = P_y/k$). Assuming that the pressure time-history is a unit impulse, the initial kinetic energy of the SDoF system is equal to ${E_k}^0 = {i_r}^2/2 \cdot m$, where $i_r$ is the reflected shock wave impulse, and $m$ is the equivalent mass of the SDoF system. The maximum potential (or hysteretic) energy, for a perfect elastic–plastic SDoF system, is reached when the system reaches its maximum displacement and is defined as follows (area under the force-displacement curve)

$$E_p^{\max} = \frac{1}{2} \cdot k \cdot {u_{\max}}^2 = \frac{1}{2} \cdot k \cdot \left(\frac{\mu \cdot P_y}{k}\right)^2 = \frac{1}{2} \cdot \frac{\left(\mu \cdot P_y\right)^2}{k}$$

$$E_p^{\max} = \frac{P_y \cdot u_{ry}}{2} \cdot (1 + 2 \cdot (\mu - 1)) = \frac{{P_y}^2}{2 \cdot k} \cdot (2 \cdot \mu - 1)$$

Assuming that there is not internal or external sources of energy dissipation, the initial kinetic energy is transformed to potential energy based on the energy conservation principle (${E_k}^0 = E_p^{\max}$). Substituting the dynamic properties used for the equivalent SDoF system into equation (2), the chamber thickness subjected to a unit impulsive can be obtained as follows

$$\begin{aligned} h &= \frac{1}{\sigma_y \cdot \mu} \cdot \sqrt{\frac{E}{2 \cdot \rho \cdot (1 - \nu)}} \cdot i_r \quad for\ \mu \leqslant 1 \\ h &= \frac{1}{\sigma_y \cdot \sqrt{2 \cdot \mu - 1}} \cdot \sqrt{\frac{E}{2 \cdot \rho \cdot (1 - \nu)}} \cdot i_r \quad for\ \mu \geqslant 1 \end{aligned} \tag{3}$$

As a result from equation (3), the ratio between the chamber thickness and the elastic thickness ($h_{elastic} = h_{\mu = 1} = h(\mu = 1)$) will depend mainly on the ductility ratio

$$\begin{aligned} \frac{h}{h_{elastic}} &= \left\{ \begin{array}{ll} 1/\mu & \mu \leqslant 1 \\ 1/\sqrt{2 \cdot \mu - 1} & \mu \geqslant 1 \end{array} \right\} \times \\ \frac{i_r[W, a - h/2]}{i_r[W, a - h_{elastic}/2]} &\approx \left\{ \begin{array}{ll} 1/\mu & \mu \leqslant 1 \\ 1/\sqrt{2 \cdot \mu - 1} & \mu \geqslant 1 \end{array} \right. \end{aligned} \tag{4}$$

The dimensionless thickness ratio, $h/h_{elastic}$ (equation (4)), normalizes the influences of several structural and geometrical parameters. That is, chambers with different mean radius ($a$), charge weights ($W$), and material properties can be compared independent of their values. In view of that, results that are shown during the following sections are presented as a function of $h/h_{elastic}$. However, $h_{elastic}$ will be later obtained using a simplified triangular pulse (Case 1S, Table 1) that reduces slightly errors on the approximation associated with the unit impulse approach.

## Simplified blast loading

The three pressure time-history components that act on the chamber walls are obtained according to the UFC guidelines, Baker's approach, and assuming that the vessel is initially full of air at normal atmospheric conditions.

### First shock wave

In this study, the first shock wave is modeled using a triangular function. The values to estimate the peak reflected pressure ($P_r$) and the reflected impulse ($i_r$) are directly obtained from the UFC Code (UFC 3-340-02, 2008).

$$\begin{aligned} &if\ \mu \leqslant 1\ (elastic) \\ &if\ \mu \geqslant 1\ (plastic) \end{aligned} \tag{2}$$

### Re-reflected shock waves

The confinement conditions associated with fully or partially confined chambers cause that the first shock wave is successively reflected on the chamber wall. The UFC approach does not consider the effect of the train of re-reflected shock waves acting on structures. However, this phenomenon increases the impulse and can produce resonance, as it is discussed later in this article.

A common approach that is used in this research assumes that the train of shock waves is modeled by three consecutive pulses considering that the peak pressure for each consecutive pulse is halved during each reflection (Baker and Kulesz, 1983; Baker et al., 1966; Smith and Hetherington, 1994). The duration of each re-reflected shock wave is assumed to be constant and equal to the duration of the first shock wave, that is, $t_{0_1} = t_{0_2} = t_{0_3} = t_0$. The approach assumes that the re-reflected shock waves propagate at the same average velocity that is observed during the first shock wave; thus, consecutive triangular pulses strike the chamber wall with an recurrence period (reverberation time)

**Table 2.** Analyzed parameters' ranges.

| Mean radius ($a$) (mm) | Range of charges ($W$) (TNT, kg) | Range of $h_{\mu=0.2}$ (mm) | Range of $h_{elastic} = h_{\mu=1}$ (mm) | Range of $h_{\mu=5}$ (mm) |
|---|---|---|---|---|
| 250 | 0.05–1.8 | 19–157 | 4–80 | 1.2–25 |
| 500 | 0.25–10 | 26–340 | 5–115 | 1.7–36 |
| 750 | 0.25–30 | 14–439 | 3–154 | 1.0–49 |
| 1000 | 0.5–50 | 15–614 | 3–150 | 1.1–48 |
| 1500 | 1–120 | 16–831 | 3–169 | 1.1–55 |
| 2000 | 2–170 | 18–1066 | 4–146 | 1.3–48 |
| 2500 | 5–300 | 28–1217 | 6–166 | 2.0–54 |
| 3000 | 10–400 | 38–1048 | 8–157 | 2.6–52 |

TNT: trinitrotoluene.

that is twice the arrival time predicted for the first shock wave ($2 \cdot t_a$, with $t_a$ estimated from the UFC curve, Figures 2 to 7). After that, the quasi-static gas pressure is assumed to be dominant and other shock waves are ignored (Edri et al., 2011). In this research, the same train of shock wave profile is assumed for chambers with and without ventilation.

## Gas pressure

The gas pressure component is originated by the confinement conditions that restrain the free expansion of the gas. The gas pressure component for partially confined chambers is commonly modeled according to a triangular (UFC 3-340-02, 2008) or an exponential decaying function (Anderson et al., 1983). In this study, the gas pressure component is determined using the UFC's approach, which is described by a triangular pulse that depends on two parameters; the peak gas pressure ($P_g$) and the equivalent gas pressure duration $t_g = 2i_g/P_g$, where $i_g$ is the gas pressure impulse.

Experimental and dimensionless analyses of partially confined vessels have shown that the peak gas pressure is independent of the ventilations (Anderson et al., 1983). Therefore, the peak gas pressure is the same for vented or unvented cases.

For the vented case, it is assumed that there is not a frangible cover ($W_F = 0$, and $i_g$ is independent of $i_r$); therefore, ventilation generates the minimum gas impulse that refers to the case that ventilation attenuates most significantly the gas pressure component. The peak gas pressure and when it occurs can be estimated based on experimental observations described by Baker (1983). That is, the gas pressure is assumed to increase linearly up to the peak vented gas pressure is reached, just at the time corresponding to the end of the reverberation phase (after the three shock waves), that is, $4 \cdot t_a + t_0$ after the first shock wave impinges the chamber wall.

## Blasting scenarios

The first aim of this study is to analyze the effect of each pressure component on the demand of ductility of spherical chamber subjected to concentric TNT detonations. The second objective is to discuss about the effect of ventilation on the reduction of the gas pressure component and its consequence in the dynamic response and corresponding damage. Taken into account these objectives, different blasting scenarios, summarized in Table 1, are considered during the course of the following sections.

All blast scenarios are solved numerically considering the equivalent perfect elastic–plastic SDoF system. Results are presented in terms of the dimensionless thickness ($h/h_{elastic}$) and the maximum ductility ratio ($\mu = u_{r-\max}/u_{ry}$, where $u_{r-\max}$ is the maximum radial displacement obtained from the numerical solution and $u_{ry} = \sigma_y \cdot a \cdot (1-\nu)/E$ is the yielding radial displacement).

Several numerical simulations (more than 25,000), related to the SDoF system, have been performed allowing to cover a wide range of combinations between parameters, which are summarized in Table 2.

The Case 1S is taken as reference for future comparisons because it displays the smallest ductility ratio and it can be easily compared with the unit impulse approach. Figure 1 shows the ductility ratio as a function of the dimensionless thickness corresponding to the load Case 1S for different charge weights (between 1 and 120 kg). These curves show that results are almost independent **of** the TNT charge weight, indicating that equation (4) is sufficiently accurate to predict the thickness for ductile systems.

The same set of parameters derived for Case 1S are then used to evaluate the performance associated with other blasting scenarios detailed in Table 1. As a result, effects of each pressure component and ventilation can be analyzed and compared.

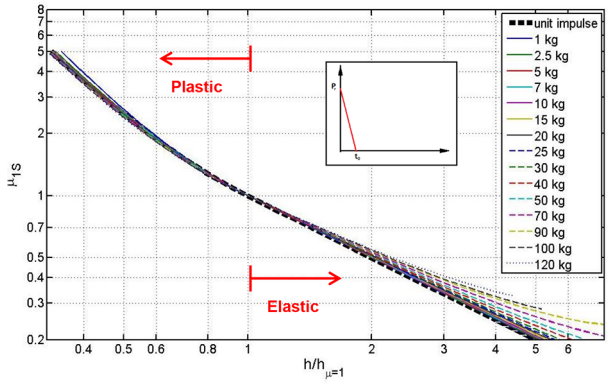


**Figure 1.** Ductility ratio for Case 1S as a function of the dimensionless thickness ($a$ = 1500 mm) for different TNT charge weights.

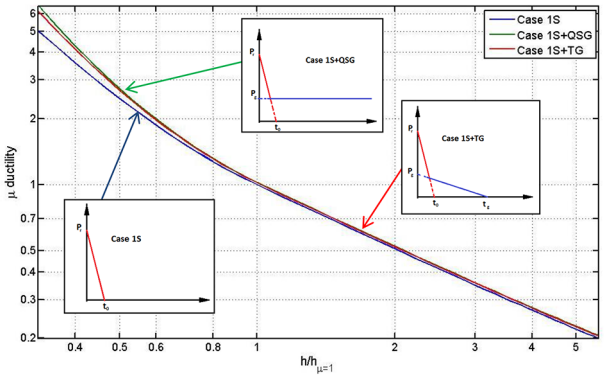


**Figure 2.** Ductility ratios for Case 1S, Case 1S + QSG, and Case 1S + TG of a spherical chamber ($a$ = 1500 mm and steel BHW35) subjected to a concentric detonation of a charge weight $W$ = 25 kg, $A_v/A_{chamber}$ = 25%, and different thicknesses.

## Effects of different blast scenarios on the chamber response

In this section, the effect of each pressure component is studied in terms of the increase in the maximum ductility ratio. To analyze the effect of each pressure component and/or ventilation, results are presented in terms of the quotient between ductility ratios obtained for two different blasting scenarios (Table 1). This quotient refers to the amplification (or deamplifications) on the demand of ductility between the compared cases (numerator/denominator). This quotient represents also the amplification ratio of the peak radial displacement between the compared cases ($\mu_1/\mu_2 = u_{r-\max-1}/u_{r-\max-2}$, where $\mu_1 = u_{r-\max-1}/u_{ry}$, $\mu_2 = u_{r-\max-2}/u_{ry}$, $u_{ry} = \sigma_y \cdot a \cdot (1-\nu)/E$, and $u_{r-\max-1}$ and $u_{r-\max-2}$ are the maximum radial displacement for Case 1 and Case 2, respectively).

### *UFC's basic pressure profiles: Case 1S, Case 1S + QSG, and Case 1S + TG*

In this section, the response of a spherical chamber subjected to the loading Case 1S, Case 1S + QSG, and Case 1S + TG are compared. Figure 2 shows the maximum ductility ratio for the three loading cases in terms of the dimensionless thickness, associated with a spherical chamber ($a$ = 1500 mm and steel BHW35) subjected to a concentric detonation of a TNT charge weight of $W$ = 25 kg and different thicknesses (14.5–244.1 mm, where $h_{elastic} = h_{\mu=1}$ = 43.7 mm).

From Figure 2, one can conclude that the gas pressure component increases the ductility ratio, especially when the chamber wall thickness is smaller than the elastic thickness. From the comparison between Case 1S + QSG and Case 1S + TG, it can be concluded that the effect of ventilation reduces slightly the ductility demand.

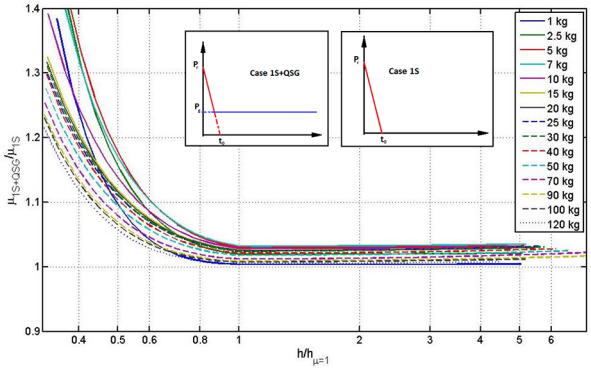


**Figure 3.** Normalized ductility ratios of Case 1S + QSG to Case 1S ($\mu_{1S+QSG}/\mu_{1S}$) as function of the dimensionless thickness for different charge weights ($a$ = 1500 mm).

Figure 3 shows the ductility ratio obtained for Case 1S + QSG is normalized by the Case 1S ($\mu_{1S+QSG}/\mu_{1S}$). From the Figure 3, one can conclude that the gas pressure component increases the ductility ratio when ductile chambers are analyzed. For example, an increment of 10% on the ductility ratio is observed when the dimensionless thickness ($h/h_{\mu=1}$) is approximately equal to 0.6.

Figure 3 shows that the peak response of elastic spherical chambers is practically insensitive to the gas pressure component; in contrast, ductile chambers show that the pressure gas component increases considerably the peak response. The pressure profiles analyzed in this section are governed by the first shock wave; hence, the chamber response is mainly impulsive. That is, the peak radial response ($u_{r-\max}$) is reached

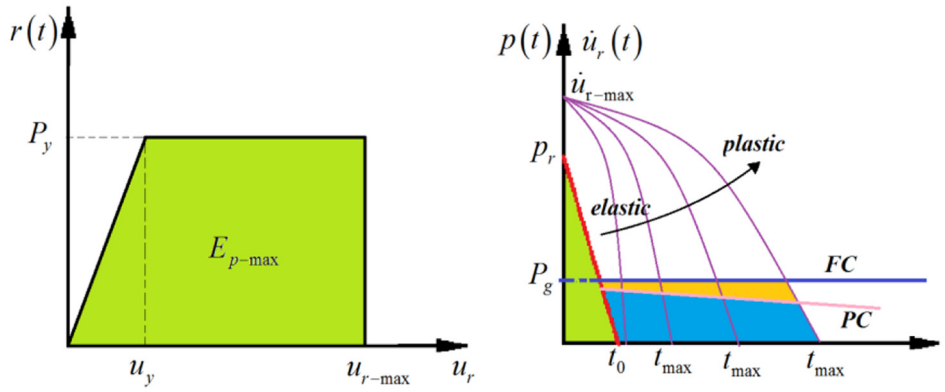


**Figure 4.** Sketch of maximum internal energy absorbed by the chamber and comparison between pressure and radial velocity for the calculation of the pressure work.

during the first cycle of the response and can be obtained assuming that the maximum potential energy ($E_{p-\max}$, Figure 4) is equal to the gas pressure work ($W_{gas}(t_{\max})$), which is done until the peak response is observed ($t_{\max}$), that is

$$E_{p-\max} = P_y \cdot \left(u_{r-\max} - u_y/2\right) = W_{gas}(t_{\max}) = \int_0^{t_{\max}} p(t) \cdot \dot{u}_r(t)dt \tag{5}$$

where $P_y = 2 \cdot h \cdot \sigma_y / a$ is the equivalent yielding pressure, $\dot{u}_r(t)$ is the radial chamber velocity, and $r(t) = k \cdot (u_r(t) - u_p(t))$ is the equivalent elastic–plastic force.

Assuming an impulsive response, the peak radial response can be obtained for Case 1S and Case 1S + QSG (or 1S + TG) as follows

$$u_{r-\max}^{1S} = \frac{1}{P_y} \cdot \left(\int_0^{t_0} p^{SW}(t) \cdot \dot{u}_r(t)dt\right) + \frac{u_{ry}}{2}$$
$$u_{r-\max}^{1S+QSG} = \frac{1}{P_y} \cdot \left(\int_0^{t_1} p^{SW}(t) \cdot \dot{u}_r(t)dt + \int_{t1}^{t_{\max}} p^{gas}(t) \cdot \dot{u}_r(t)dt\right) + \frac{u_{ry}}{2} \tag{6}$$

where $t_1$ is the time when the gas pressure becomes dominant, that is, $p^{gas}(t) \geq p^{SW}(t)$, $p^{gas}(t)$ is the gas pressure component (equal to $P_g$ for Case 1S + QSG) and $p^{SW}(t)$ is the pulse pressure associated with the first shock wave (Case 1S). If we assume that there is not a significant difference of $\dot{u}_r(t)$ when $t \in [t_1, t_0]$ associated with both cases, then normalized ductility between Case 1S + QSG and Case 1S can be calculated as follows

$$\frac{\mu_{1S+QSG}}{\mu_{1S}} = \frac{u_{r-\max}^{1S+QSG}}{u_{r-\max}^{1S}} \approx 1 + \frac{\int_{t_1}^{t_{\max}} \left[p^{gas}(t) - p^{SW}(t)\right] \cdot \dot{u}_r(t)dt}{\int_0^{t_0} p^{SW}(t) \cdot \dot{u}_r(t)dt + \frac{u_{ry} \cdot P_y}{2}} \tag{7}$$

When an SDoF system is subjected to a short-duration pulse, the peak radial velocity is observed during the initial phase of the response (Figure 4). After that, the peak radial displacement will occur when the radial velocity becomes zero ($t = t_{\max}$).

One can observe from Figure 4 that the peak response for elastic chambers is rapidly reached (i.e. $t_{\max} \approx T_n/4$), due to the high natural frequency associated with the RBM. In contrast, the peak response is reached later ($t_{\max}$) when the chamber responds plastically, owing that the secant RBM frequency is consequently reduced. Therefore, the gas pressure impulse that contributes to amplify the peak response ($\int_{t_1}^{t_{\max}} [p^{gas}(t) - p^{SW}(t)]dt$, blue and orange areas of Figure 4) becomes smaller as the chamber tends to response elastically. Similarly, the radial velocity that is observed when the pressure gas component becomes dominant ($t > t_1$) is smaller while the chamber does not respond plastically (Figure 4).

The right term of equation (7) refers to the ratio between the gas pressure work that is done by the gas pressure component until the peak response is reached and the pressure work that is done by the first shock wave. This ratio is small for elastic systems because the gas pressure pulse that contributes to the peak response is low and the radial velocity ($\dot{u}_r(t)$) is also low when $t > t_1$. However, this ratio becomes significant when the chamber behaves plastically, which explain why the gas pressure component increases the ductility ratio.

Figure 5 shows ductility ratios obtained for Case 1S + TG (partially confined) normalized by those of

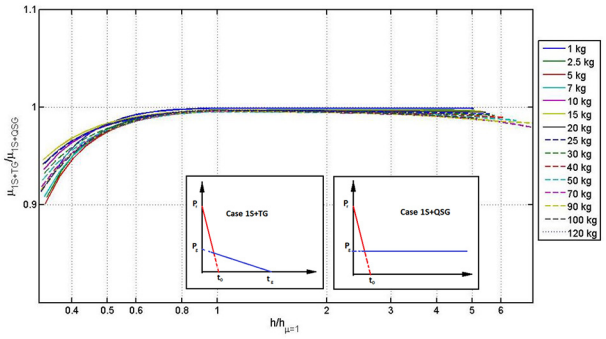


**Figure 5.** Normalized ductility ratios for Case 1S + TG and Case 1S + QSG ($\mu_{1S+TG}/\mu_{1S+QSG}$) as function of $h/h_{elastic}$ for different charge weights ($a$ = 1500 mm).

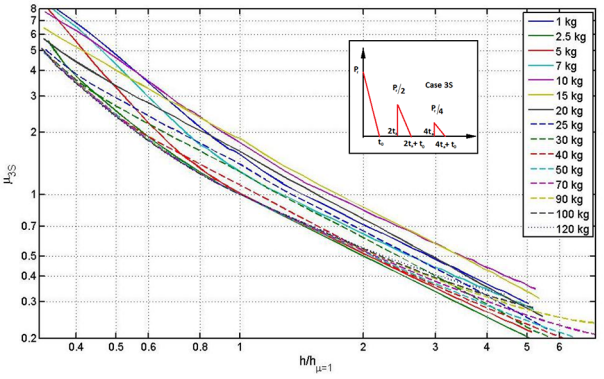


**Figure 6.** Ductility ratios of Case 3S for several dimensionless thicknesses and charge weights ($a$ = 1500 mm).

Case 1S + QSG (fully confined), respectively ($\mu_{1S+TG}/\mu_{1S+QSG}$). From this figure, the ductility reduction due to ventilation is explained. To sum up, ventilation generates an insignificant reduction on the ductility demand (or maximum displacement) for linear systems ($h/h_{\mu=1} \geq 1$). Similarly, the reduction of the peak response for non-linear chambers is limited for ductile systems. For example, the maximum ductility reduction is smaller than 10% for $\mu \leq 5$. From Figure 5, one can observe that the obtained curves indicate that the ductility reduction due to ventilation could be significant for system that shows vary high ductility demands ($\mu > 5$).

The ineffectiveness of ventilation to reduce the peak chamber response can be explained by rewriting equation (7). That is, the normalized ductility between Case 1S + QSG and the Case 1S + TG can be obtained assuming that the radial velocity ($\dot{u}_r(t)$) is not significantly modified between these cases, and expressed as follows

$$\frac{\mu_{1S+TG}}{\mu_{1S+QSG}} = \frac{u_{r-\max}^{1S+TG}}{u_{r-\max}^{1S+QSG}} \approx 1 - \frac{\int_{t_1}^{t_{\max}} \left[p_{1S+QSG}^{gas}(t) - p_{1S+TG}^{gas}(t)\right] \cdot \dot{u}_r(t)dt}{\int_0^{t_{\max}} p_{1S+TG}(t) \cdot \dot{u}_r(t)dt + \frac{u_y \cdot P_y}{2}} \quad (8)$$

The reduction of ductility because of ventilation is related to the second term of equation (8). The numerator refers to the gas pressure work that is done by the difference between the gas pressure components obtained for Case 1S + QSG and Case 1S + TG, respectively. In general, this value is low because the impulse associated with the difference between the gas pressure profiles ($\int_{t_1}^{t_{\max}} [p_{1S+QSG}^{gas}(t) - p_{1S+TG}^{gas}(t)]dt$, orange area of Figure 4) tends to be small and because the radial velocity is also negligible when the larger

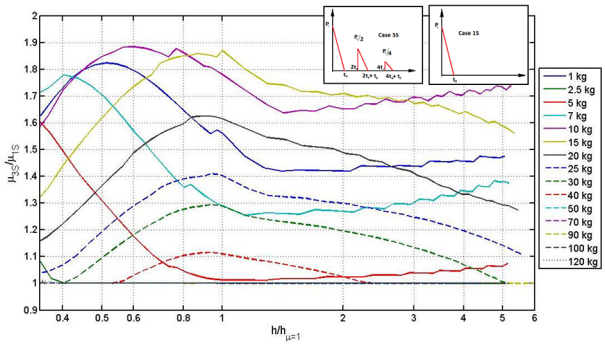


**Figure 7.** Normalized ductility ratio of Case 3S to Case 1S for several dimensionless thicknesses and charge weights ($a$ = 1500 mm).

differences between these gas pressure components becomes significant (Figure 4). Moreover, the denominator of equation (8) refers to the total gas pressure work associated with Case 1S + TG (green, blue, and orange areas in Figure 4); therefore, the numerator is normalized by a high value. It can be concluded that the second term of equation (8) tends to be small if the chamber does not display a substantial plastic response.

## *Effect of re-reflected shock waves*

The effect of re-reflected shock waves is analyzed based on the comparison between the maximum ductility ratio obtained for Case 1S and Case 3S. Figure 6 shows the ductility ratio for Case 3S associated with a spherical chamber ($a$ = 1500 mm and steel BHW35) subjected to a set of different TNT charge weights (1–120 kg). From the comparison between Figures 1 and 6, one can observe that the re-reflected shock waves increase significantly the ductility demand.

Figure 7 shows the normalized ductility ratio obtained between the Case 3S and Case 1S. This

normalized ratio refers to the amplification generated by re-reflected pulses. From Figure 7, one can conclude that (1) both elastic and plastic chambers show amplification; (2) the maximum amplification of ductility ratio is 1.85 (see Appendix 1); (3) the amplification depends on the equivalent TNT charge weight, the chamber wall thickness, and the chamber radius; (4) plastic chambers are more susceptible to amplifications; and (5) the train of re-reflected shock waves plays an important role and should be considered for design of blast chambers.

The amplification caused by re-reflected shock waves (Figure 7) is not described exclusively by the ratio between the chamber natural frequency and the frequency of pulses, as the elastic theory predicts. This fact is observed because Figure 7 shows that the amplification vary strongly with the chamber wall thickness (or dimensionless thickness value). However, the chamber natural frequency is invariant with the thickness; similarly, the reverberating time of re-reflected pulses ($2 \cdot t_a$) depends mainly on the TNT charge weight and the chamber radius. Therefore, one could expect a constant amplification for each combination between TNT charge weight and chamber radius (i.e. a constant curve with the dimensionless thickness) when elastic theory is employed. Therefore, one can conclude that the amplification that is generated by re-reflected shock waves depends on the scale of the problem.

Spherical chambers subjected to concentric detonation are described by the RBM, which is related to a high natural frequency. In general, the RBM frequency is comparable with the reverberating frequency of re-reflected shock waves. Therefore, the radial response shows a vibratory response between each re-reflected shock wave. This vibratory response is amplified by secondary re-reflected shock waves as soon as these secondary pulses coincide with a positive radial velocity, that is, they cause a resonance response.

The maximum potential energy (if dissipation sources are ignored) for a SDoF system subjected to a train of three pulses (with a duration $t_0$ and a reverberating time $2 \cdot t_a$) can be estimated by equaling this energy with the gas pressure work that is done by the three pulses

$$E_{p-\max} = \begin{cases} \int_0^{t_0} p(t) \cdot \dot{u}_r(t) dt & \forall t_0 < t \leq 2 \cdot t_a \\ \int_0^{t_0} p(t) \cdot \dot{u}_r(t) dt + \int_{2 \cdot t_a}^{2 \cdot t_a + t_0} p(t) \cdot \dot{u}_r(t) dt & \forall 2 \cdot t_a + t_0 < t \leq 4 \cdot t_a + t_0 \\ \int_0^{t_0} p(t) \cdot \dot{u}_r(t) dt + \int_{2 \cdot t_a}^{2 \cdot t_a + t_0} p(t) \cdot \dot{u}_r(t) dt + \int_{4 \cdot t_a}^{4 \cdot t_a + t_0} p(t) \cdot \dot{u}_r(t) dt & \forall 4 \cdot t_a + t_0 < t \end{cases} \quad (9)$$

Figure 8 shows the hysteretic curve, that is, the equivalent elastic–plastic force ($r(t)$) is plotted versus

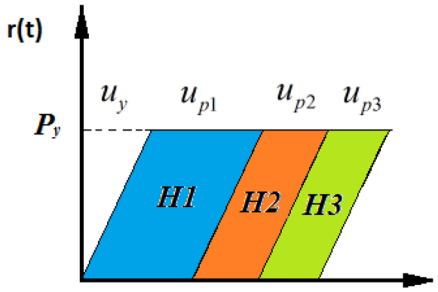


**Figure 8.** Sketch of energy contribution associated with each pulse (assuming that shock wave coincide with a positive radial velocity).

the radial displacement ($u_r(t)$), where $r(t) = k \cdot (u_r(t) - u_p(t))$ and $k = 2 \cdot h \cdot E/(1-\nu) \cdot a^2$, and $u_p(t)$ the accumulated plastic radial displacement. Based on the energy conservation principle, the hysteretic energy is equal to the maximum potential energy ($E_{p-\max}$). Therefore, the increase in the hysteretic energy related to each pulse (areas H1, H2, and H3 of Figure 8) is equal to the increase in the maximum potential energy ($E^{(1)}_{p-\max}, E^{(2)}_{p-\max}$, and $E^{(3)}_{p-\max}$).

If we assume that each pulse can be modeled such as a unit impulse, then we can obtain an upper limit for the energy contribution associated with each pulse as follows (see Appendix 1)

$$\begin{aligned} E^{(1)}_{p-\max} &= H1 + \frac{u_{ry} \cdot P_y}{2} = \int_0^{t_0} p(t) \cdot \dot{u}_r(t) dt \leq \frac{1}{2} \frac{i_r^2}{m} \\ E^{(2)}_{p-\max} &= H2 = \int_{2 \cdot t_a}^{2 \cdot t_a + t_0} p(t) \cdot \dot{u}_r(t) dt \leq \frac{1}{2} \frac{i_{r-2}^2}{m} + i_{r-2} \cdot \dot{u}_r(2 \cdot t_a) \\ E^{(3)}_{p-\max} &= H3 = \int_{4 \cdot t_a}^{4 \cdot t_a + t_0} p(t) \cdot \dot{u}_r(t) dt \leq \frac{1}{2} \frac{i_{r-3}^2}{m} + i_{r-3} \cdot \dot{u}_r(4 \cdot t_a) \\ &\text{where } i_{r-2} = \frac{i_r}{2}; i_{r-3} = \frac{i_r}{4} \text{ and } m = \rho \cdot h \end{aligned} \quad (10)$$

If the peak radial displacement occurs after that each pulse has finished, the vibratory response is

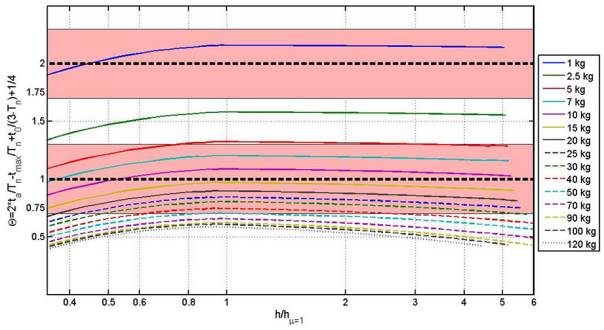


**Figure 9.** $\Theta = ((2 \cdot t_a)/T_n) + (t_0/(3 \cdot T_n)) - (t_{max}/T_n) + (1/4)$ versus $h/h_{elastic}$ corresponding to different charge weights ($a$ = 1500 mm).

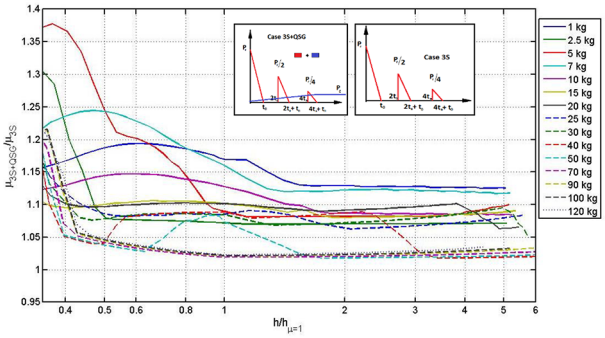


**Figure 10.** Normalized ductility ratios (Case 3S + QSG to Case 3S) as a function of the dimensionless thickness ($a$ = 1500 mm) for different charge weights (1–120 kg).

described by $u_r(t) = u_{r\max} \cdot \cos(\omega_n \cdot (t - t_{\max}))$. Therefore, the condition for the maximum contribution of the subsequent pulse can be derived assuming that the center of gravity of the subsequent pulse coincides with the peak positive radial velocity

$$2 \cdot t_a + \frac{t_0}{3} = t_{\max} + \frac{3}{4} \cdot T_n + T_n \cdot (n-1) \quad \forall n = 1, \ldots, \infty$$
$$\Rightarrow \Theta = \frac{2 \cdot t_a}{T_n} + \frac{t_0}{3 \cdot T_n} - \frac{t_{\max}}{T_n} + \frac{1}{4} = n \quad \forall n = 1, \ldots, \infty \tag{11}$$

Therefore, the amplification factor ($\mu_{3S}/\mu_{1S}$, Figure 7), for perfect elastic–plastic systems, does not depend on $2 \cdot t_a/T_n$ such the linear theory predicts; instead, numerical results show that the amplification occurs when $\Theta \in [0.7 - 1.3]$ or $[1.7 - 2.3]$ (pink areas of Figure 9). Figure 9 shows $\Theta$ against the dimensionless thickness, which is highly correlated with the amplification factor ($\mu_{3S}/\mu_{1S}$, Figure 7), that is, $\mu_{3S}/\mu_{1S} \approx f(\Theta)$. From comparison between Figures 7 and 9, one can observe that the maximum amplification factor (1.85, Figure 7) occurs when $\Theta$ is close to 1.0 or 2.0, and $\mu_{3S}/\mu_{1S}$ is reduced when $\Theta$ is far-off 1.0 or 2.0.

From Figures 7 and 9, one can conclude that the amplification due to resonance is not observed for some cases (e.g. $W$ = 2.5 kg or $W \geqslant$ 50 kg, Figure 7) because the re-reflected pulses impinge the chamber walls when the radial velocity is negative. If a nonlinear response occurs, $t_{\max}$ will depend strongly on the chamber thickness. This explains why plastic resonance depends on the chamber thickness and the scale of the problem. For linear systems, $t_{\max} \approx T_n/4$ (unit impulse assumption), which makes that equation (11) is coincident with the classic elastic theory.

The appendix shows a simplified approach to estimate the maximum ductility ratio, assuming that the blast loading is described by three unit impulses and all of them coincide with a peak positive radial velocity (plastic resonance approach).

## *Effect of gas pressure and ventilation when the three simplified pressure components are considered*

In this section, the effect of the gas pressure component and ventilation is analyzed, considering the superposition of the three pressure components. The comparison between Case 3S and Case 3S + QSG allows understanding the effect of the gas pressure component and the comparison between Case 3S + TG and Case 3S + QSG is employed to analyze the effect of ventilation.

Figure 10 shows ductility ratios calculated for case 3S + QSG normalized by those from Case 3S. This figure shows the effect of the gas pressure component when shock waves are taken into account. From Figure 10, one can conclude that the gas pressure component can increase significantly the ductility ratio until 40% (and 15% for elastic chambers) in comparison with the case when it is ignored.

Figure 11 shows the normalized ductility ratio between the case 3S + TG (partially confined chamber with 10% of effective vented area) and the case 3S + QSG (fully confined chamber). From Figure 11, it can be concluded that opening/frangible covers (with an effective vent area equivalent to 10% or lower) allow reducing the ductility demand up to 5% in comparison to fully confined chambers.

These analyses were repeated using different material properties and chamber radiuses, finding the same overall results (which are not presented due to page limitation). Similarly, the analysis was executed using a significant opening area of 20%, showing that this ventilation can reduce the ductility ratio by 15% (maximum reduction), and just 5% for most of the cases.

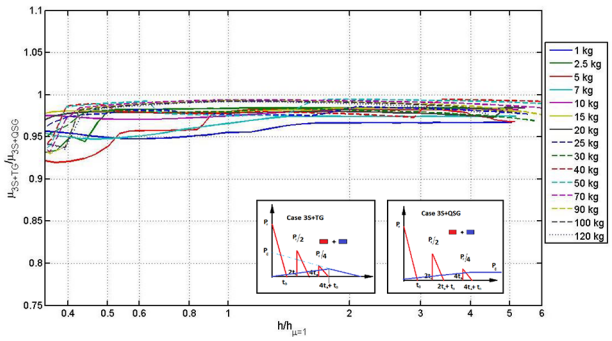


**Figure 11.** Normalized ductility ratios (Case 3S + TG ($A_v$/$A_{chamber}$ = 10%) to Case 3S + QSG) for a spherical chamber ($a$ = 1500 mm) with different dimensionless thicknesses and TNT charge weights (1–120 kg).

## Comments and results discussion

Dynamic responses of spherical chambers are governed by the RBM, which is associated with very high natural frequencies. In fact, spherical chambers show a vibratory response between each consecutive re-reflected shock wave. Therefore, spherical chambers are susceptible to plastic (or elastic) resonance when the re-reflected pulses coincide with positive radial velocities.

The gas pressure component is related to a monotonically decreasing or a constant function (partially confined or fully confined chambers). Therefore, the work that is done by the gas pressure component during one cycle of vibration is canceled if the chamber shows an harmonic response, that is, the gas work will be null as soon as the peak positive velocity is similar to the peak negative velocity and the gas pressure remains constant. Nevertheless, if plastic resonance occurs (because re-reflected shock waves), the positive velocity will be higher than the negative velocity causing that the gas work that is done by the gas pressure component increase the chamber deformation.

Natural frequencies of chambers with other geometries that contain flat walls, such as cubical chambers, are significantly lower than the obtained for membrane vessels (because they display an initial flexural response rather than a membrane behavior). Thus, the chamber response of flexural members is not described by a vibratory response between shock waves; instead, it is described by a damped harmonic oscillation. For these cases, the peak chamber response is related to the impulse that is observed until the peak response is reached, that is, the maximum ductility ratio is controlled by the pressure time-history that is observed until the first peak response is reached. If the natural period of the chamber is higher (e.g. $T_n > 4 \cdot (4 \cdot t_a + t_0)$), the influence of the gas pressure impulse becomes important and can increase significantly the structural response. Hence, ventilation should be an effective tool to mitigate the impulse and improve the performance of chambers with flat walls.

In this article, we have studied spherical chambers that display a ductility ratio smaller than 5.0 (for Case 1S). However, other blasting scenarios that include additional pressure components reach ductility ratios values as high as 8.0. From the presented analysis, we have concluded that ventilation is an ineffective tool to mitigate damage of spherical blast chambers; however, ventilation could be effective if higher ductility ratios are allowed (higher than 8.0) according to the trend that is observed in Figure 11. In general, it is not recommended to use ductility ratios higher than 8.0 when an explosive chamber is designed, especially if brittle materials (e.g. steels with high yielding strength) are used for the design of membrane blast pressure vessel.

The effects of eccentric detonations have not been discussed in this article because the limitations of the SDoF approach. Similarly, other important design aspects have not been analyzed in this article. One of them is the effect of temperature. In general, the effect of temperature is traditionally ignored when structures are subject to HE explosions, owing that the pressure profiles last few milliseconds and structure provides enough ventilation to avoid long-term effects associated with the confinement. However, fully confined chambers show a quasi-static pressure that can last several minutes (or hours) before that it is dissipated by thermal convection through the chamber walls or released from a venting device. The quasi-static gas pressure is triggered because the chemical energy allocated in the HE is transformed to internal energy that causes a residual constant pressure and temperature. In fact, Edri et al. (2013) derived that the final temperature of the gas mixture is a function of the charge weight density. Finding that the quasi-static temperature of the gas mixture is higher than 2300°C when $W/V > 0.0241$ lb/ft$^3$ for confined TNT explosions (observing that the forging temperature for carbon steels is approximately 1230°C and the melting point is around to 1400°C). Therefore, a fully confined chamber should be also able to resist the combined effect between the quasi-static gas pressure and temperature. However, ventilation allows a relatively fast release of the QS gas pressure and temperature; therefore, temperature effect can be potentially ignored when ventilation is provided. In conclusion, this second design aspect could make mandatory to use ventilation because it allows reducing the final gas mixture temperature.

Another aspect that has not been considered in this article refers to the mitigation of the re-reflected shock waves. Here, the re-reflected shock waves have been

estimated by three re-reflected pulses according to Baker's approach (Baker and Kulesz, 1983). However, computational fluid dynamics (CFD) simulations and experimental data (Buzukov, 1980) have shown that re-reflected shock waves are not necessarily quickly attenuated; therefore, the number of significant re-reflected shock waves could be more than three pulses. CFD simulations indicate that secondary shock waves propagate slower than the first shock wave; thus, the reverberating time is longer than the value assumed by the simplified approach in (Baker and Kulesz, 1983). As a result, elastic or plastic resonance could not occur at the same conditions that have been derived in this article. Moreover, a slow shock wave attenuation and the implication of extra powerful re-reflected shock waves can generate significant plastic resonance (when they coincide with positive radial velocities).

In this article, we have assumed that re-reflected shock waves are not significantly attenuated by small openings because only three pulses were considered. Nevertheless, ventilation could be effective to mitigate re-reflected shock waves when multiple shocks (more than three) are observed, that is, ventilation can be effective to reduce the plastic resonance phenomenon when multiple shock waves are displayed.

Finally, another aspect related to mitigation of re-reflected shock waves is associated with the chamber geometry and the relative position of the vent respect to the detonation point. A significant mitigation of re-reflected shock waves can be initially achieved if the first shock wave is orientated toward the opening direction.

## Conclusion

The effect of each pressure component on the ductility demand of spherical chambers subjected to concentric TNT spherical explosions have been studied using a simplified equivalent SDoF approach. It is shown that the three pressure components contribute significantly to the response. Therefore, all of them should be considered when vessels are designed to resist fully or partially confined HE explosions.

The results have been presented in terms of a dimensionless thickness (which is justified by a unit impulse approach) and the dimensionless quotient between ductility ratios obtained between two different blast scenarios. This allows comparing the effect of each component independent of the scale of the problem.

The inclusion of two subsequent re-reflected shock waves can cause elastic or plastic resonance, which could amplify the chamber response and ductility ratio by a factor of 1.85. The amplification generated by re-reflected shock waves depends on the scale of the problem for ductile systems.

The plastic or elastic resonance phenomenon was explained and a simplified approach was proposed as an upper limit of the demand of ductility (assuming three re-reflected pulses). It is proposed to use this simplified approach for design of spherical chambers, because uncertainties associated with the reverberating time and the actual TNT charge weight can be conservatively taken into account; however, the effect of multiple shock waves (more than three) should be analyzed.

The gas pressure component can increase significantly the chamber responses around of 15% (or more). However, the common understanding that ventilation is effective to mitigate damage of storage chambers is not exactly correct. In fact, results obtained from the SDoF approach indicates that a venting area of 10% led only to a maximum of 5% reduction on the chamber response.

Spherical chambers are related to high RBM frequencies that involve a vibratory response between each consecutive shock wave. This effect generates that spherical chambers are susceptible to resonance and are not significantly affected by the long-term impulse generated by the gas pressure component.

This research has been focused on the study of the effect of ventilation on the response of spherical chambers during its dynamic response. Other design aspects such as the final gas mixture temperature or the attenuation of several powerful shock waves can make the ventilation effective and mandatory for design of vessels subjected to confined HE detonations.

### Declaration of Conflicting Interests

The author(s) declared no potential conflicts of interest with respect to the research, authorship, and/or publication of this article.

### Funding

The author(s) disclosed receipt of the following financial support for the research, authorship, and/or publication of this article: The authors acknowledge partial financial supports from Australian Research Council (ARC) and GexCon Australia Pty Ltd under ARC Linkage Project LP130100919 for carrying out this research. The first author acknowledges the Chilean government for providing scholarship for him to pursue PhD study in Australia. The authors acknowledge iVEC for providing support and access to run AUTODYN's simulations on their HPC and acknowledge the support from China National 973 project 2015CB058003 for carrying out field blasting tests for this project.

### ORCID iD

Francisco Hernandez https://orcid.org/0000-0002-3723-5394

## References


Abakumov AI, Egunov VV, Ivanov AG, et al. (1984) Calculation and experiments on the deformation of explosion-chamber shells. *Journal of Applied Mechanics and Technical Physics* 25(3): 455–458.

Adishchev VV and Kornev VM (1979) Calculation of the shells of explosion chambers. *Combustion, Explosion and Shock Waves* 15(6): 780–784.

Anderson CE, Baker WE, Wauters DK, et al. (1983) Quasi-static pressure, duration, and impulse for explosions (e.g. HE) in structures. *International Journal of Mechanical Sciences* 25(6): 455–464.

Baker WE (1960) The elastic-plastic response of thin spherical shells. *Journal of Applied Mechanics* 27(4): 139–144.

Baker WE and Allen FJ (1958) The response of elastic spherical shells to spherically symmetric internal blast loading. In: *Third U.S. national congress of applied mechanics*, Providence, RI, 11–14 June, pp. 79–87. New York: ASME.

Baker WE and Kulesz PCJ (1983) *Explosion Hazards and Evaluation*. Saint Louis, MO: Elsevier.

Baker WE, Hu WCL and Jackson TR (1966) Elastic response of thin spherical shells to axisymmetric blast loading. *Journal of Applied Mechanics: Transactions of the ASME* 334(4): 800–806.

Baker WE, Cox PA, Westine PS, et al. (1983) *Explosion Hazards and Evaluation*. New York: Oxford.

Belov AI, Belyaev VM, Kornilo VA, et al. (1986) Calculation of wall loading dynamics in a spherical combustion chamber. *Combustion, Explosion and Shock Waves* 21(6): 132–135.

Beshara FBA (1994) Modelling of blast loading on above-ground structures—II. Internal blast and ground shock. *Computers and Structures* 51(5): 597–606.

Bradley D and Mitcheson A (1978) The venting of gaseous explosions in spherical vessels. II—theory and experiment. *Combustion and Flame* 32: 237–255.

BS EN 14494:2007 (2007) Gas explosion venting protective systems.

Buzukov AA (1980) Forces produced by an explosion in an air-filled explosion chamber. *Combustion Explosion and Shock Waves* 16(5): 555–559.

Chan PC and Klein HH (1994) A study of blast effects inside an enclosure. *Journal of Fluids Engineering* 116(3): 450–456.

Chippett S (1984) Modeling of vented deflagrations. *Combustion and Flame* 55(2): 127–140.

Chopra A (1995) *Dynamics of Structures*. Upper Saddle River, NJ: Prentice Hall.

Donahue L, Zhang F and Ripley RC (2013) Numerical models for afterburning of TNT detonation products in air. *Shock Waves* 23(6): 559–573.

Dong Q, Hu BY, Chen SY, et al. (2012) Engineering design of a multiple-use spherical explosion containment vessel subjected to internal blast loading from 25 kg TNT high explosive. *Journal of Pressure Vessel Technology* 134: 021205.

Eckhoff R (2013) *Explosion Hazards in the Process Industries*. Houston, TX: Gulf Publishing Company.

Edri I, Feldgun VR, Karinski YS, et al. (2013) Afterburning aspects in an internal TNT explosion. *International Journal of Protective Structures* 4(1): 97–116.

Edri I, Savir Z, Feldgun V, et al. (2011) On blast pressure analysis due to a partially confined explosion: I. Experimental studies. *International Journal of Protective Structures* 2(1): 1–20.

Hernandez F, Abdel-jawad M and Hao H (2015) Simplified multiple equations' inverse problem of vented vessels subjected to internal gas explosions. *Journal of Loss Prevention in the Process Industries* 35: 65–79.

Hernandez F, Hao H and Abdel-Jawad M (2016) Additional afterburning energy value to simulate fully confined trinitrotoluene explosions. *International Journal of Protective Structures* 7(2): 232–264.

Karpp RR, Duffey TA and Neal TR (1983) Response of containment vessels to explosive blast loading. *Journal of Pressure Vessel Technology* 105(1): 23–27.

Li QM, Dong Q and Zheng JY (2008) Strain growth of the in-plane response in an elastic cylindrical shell. *International Journal of Impact Engineering* 35(10): 1130–1153.

Molkov V, Dobashi R, Suzuki M, et al. (2000) Venting of deflagrations: hydrocarbon-air and hydrogen-air systems. *Journal of Loss Prevention in the Process Industries* 13(3): 397–409.

Molkov VV, Grigorash AV, Eber RM, et al. (2004) Vented gaseous deflagrations: modelling of hinged inertial vent covers. *Journal of Hazardous Materials* 116(1): 1–10.

NFPA 68 (2007) Standard on explosion protection by deflagration venting. *National Fire Protection Association*. Available at: http://www.nfpa.org/

Puttock JS, Yardley MR and Cresswell TM (2000) Prediction of vapour cloud explosions using the SCOPE model. *Journal of Loss Prevention in the Process Industries* 13(3): 419–431.

Smith PD and Hetherington JG (1994) *Blast and Ballistic Loading of Structures*. Oxford: Butterworth-Heinemann.

UFC 3-340-02 (2008) *Structures to Resist the Effects of Accidental Explosions* (Structures Congress 2011). Washington, DC: Unified Facilities Criteria, Department of Defense.

White JJ III and Trott B (1980) Scaling law for the elastic response of spherical explosion-containment vessels. *Experimental Mechanics* 20(5): 174–177.

White JJ III, Trott BD and Backofen JE Jr (1977) The physics of explosion containment. *Physics in Technology* 8(3): 94–100.

Yao C, Bajpai SN and Buckley J (1969) *Evaluation of Protection from Explosion Overpressure in AEC Gloveboxes*. Norwood, MA: Factory Mutual Research Corporation.

Zhdan SA (1981) Dynamic load acting on the wall of an explosion chamber. *Combustion Explosion and Shock Waves* 17(2): 241–244.


## Appendix I

### *Plastic resonance approach (upper limit)*

A simplified approach to estimate the maximum ductility demand is described in this appendix. This approach assumes that the blast loading is described

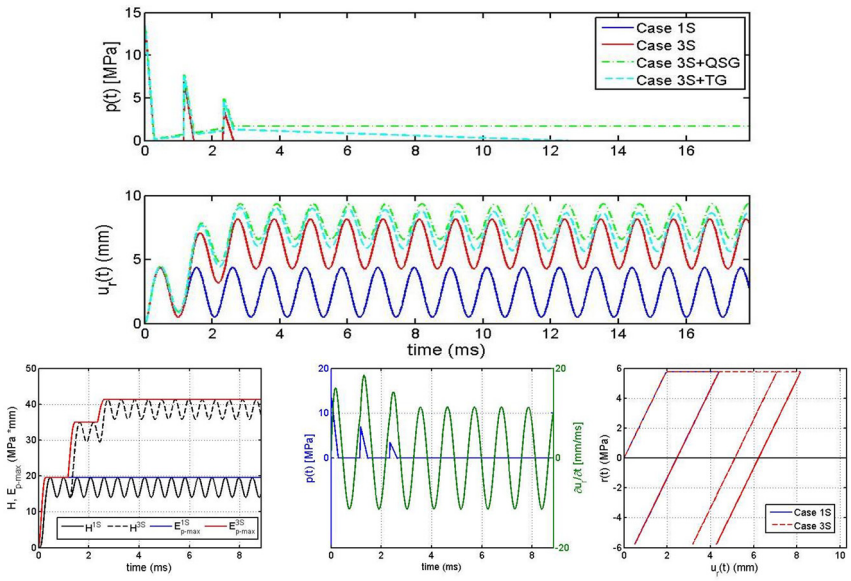


**Figure 12.** Pressure time-history; radial response ($A_v/A_{chamber}$ = 10% for 3S + TG); and hysteretic and internal pressure work (Case 1S and Case 3S), internal pressure and radial velocity (Case 3S), and hysteretic diagram (Case 1S and 3S).

by three unit impulses that coincide with peaks radial velocity (plastic resonance).

In order to demonstrate the accuracy of this approach, the case associated with plastic resonance presented in Figures 7 and 9 is analyzed. This example refers to a spherical chamber ($a$ = 1500 mm) subjected to a concentric spherical detonation of a TNT charge weight of $W$ = 10 kg. The impulse of the first shock wave is then estimated to be $i_r$ = 1.9801 MPa from the UFC 3-340-02 (2008). The chamber wall thickness is selected as $h$ = 11.0611 mm, which corresponds to $h/h_{\mu=1}$ = 0.5322 (related to plastic resonance, $\Theta$ = 1 in Figure 9, and $\mu_{3S}/\mu_{1S} \approx 1.85$ from Figure 7).

The same material properties are used in the analysis. Therefore, the SDoF dynamic properties are $m = \rho \cdot h = 0.0863\ \text{MPa} \cdot \text{ms}^2/\text{mm}$, $k = 2 \cdot h \cdot E/((1-\nu) \cdot a^2) = 2.963\,\text{N/mm}$, $P_y = 2 \cdot h \cdot \sigma_y/a = 5.752\,\text{MPa}$, $u_{ry} = P_y/k = 1.941\,\text{mm}$, $\omega_n = \sqrt{k/m} = 5861\,\text{rad/s}$ (or $T_n = 1.07\,\text{ms}$).

The tops figures in Figure 12 shows the pressure time-history and radial response for Case 1S, Case 3S, Case 3S + QSG, and Case 3S + TG that have been obtained numerically using Newmark's numerical integration method. Figure 12 shows three plots related to the numerical solution of the problem for Case 1S and Case 3S. The first plot shows the hysteretic energy ($H = \int r(u_r)\partial u_r$) and the work that is done by the internal pressure ($E_{p-\max} = \int p(t) \cdot \dot{u}_r(t)\partial t$). The second plot shows the pressure time-history and the radial chamber velocity for Case 3S (used for calculation of $E_{p-\max}$). The third plot shows the hysteretic diagram, that is, $r(t) = k \cdot (u_r(t) - u_p(t))$ against $u_r(t)$ (used for calculation of the hysteretic energy, $H$).

From Figure 12, we can conclude that the plastic resonance occurs when pulses coincide with a peak positive radial velocity (second plot) that increases the plastic work when the re-reflected pulses impinge the chamber walls (H1, H2, and H3, third plot of Figure 8). From Figure 12, it is also confirmed that the hysteretic energy is described and equal to the envelope of the internal pressure energy work (first plot).

After that, the numerical solution of the problem have been calculated when the plastic resonance occurs (Case 3S). The unit impulse approach can be used to estimate the upper limit of the ductility demand of the problem. Thus, results from the unit impulse approach can be compared with the numerical results displayed in Figure 12, which will be shown in parenthesis "()" during following calculations for comparison. The maximum internal energy related to the first shock wave is estimated from equation (10) as follows

$$E_{p-\max}^{(1)} = \frac{1}{2} \cdot \frac{i_r^2}{m} = 22.7\ \text{MPa} \cdot \text{mm}\ (19.6\ \text{MPa} \cdot \text{mm}) \tag{12}$$

If we assume that $H1 = E_{p-\max}^{(1)}$, we can obtain the plastic radial displacement that is generated by the first shock wave ($u_{p1}$, Figure 8), which is described as follows

$$u_{p1} = \frac{H1 - H_{elast}}{P_y} = 2.98 \text{ mm } (2.438 \text{ mm}),$$
$$\text{with } H_{elast} = \frac{P_y \cdot u_{ry}}{2} = 5.582 \text{ MPa} \cdot \text{mm} \quad (13)$$

The maximum radial displacement after the first shock wave is $u_{p1} + u_{ry} = 4.921$ mm (4.378 mm). Thus, the maximum ductility ratio for Case 1S is $\mu_{1S} = (u_{p1} + u_{ry})/u_{ry} = 2.535$ (2.256).

The maximum radial velocity for a perfect elastic–plastic system (after yielding) is $\dot{u}_{r-\max} = \omega_n \cdot u_{ry} = 11.375$ mm/ms (11.35 m/s); therefore, the maximum internal energy related to the second shock wave is estimated from equation (10) as follows

$$E^{(2)}_{p-\max} = \frac{1}{2} \cdot \frac{{i_r}^2}{4 \cdot m} + \frac{i_r}{2} \cdot \dot{u}_{r-\max} = (5.6 + 11.3) = 16.9 \text{ MPa} \cdot \text{mm } (15.4 \text{ MPa} \cdot \text{mm}) \quad (14)$$

Assuming that $H2 = E^{(2)}_{p-\max}$, we can obtain the plastic radial displacement related to the second shock wave ($u_{p2}$, Figure 8) as follows

$$u_{p2} = \frac{H2}{P_y} = 2.946 \text{ mm } (2.681 \text{ mm}) \quad (15)$$

The maximum radial displacement after the second shock wave is $u_{p1} + u_{p2} + u_{ry} = 7.867$ mm (7.036 mm). The maximum internal energy related to the second shock wave is obtained from equation (10) as follows

$$E^{(3)}_{p-\max} = \frac{1}{2} \cdot \frac{{i_r}^2}{16 \cdot m} + \frac{i_r}{4} \cdot \dot{u}_{r-\max} = (1.4 + 5.6) = 7.05 \text{ MPa} \cdot \text{mm } (6.33 \text{ MPa} \cdot \text{mm}) \quad (16)$$

If $H3 = E^{(3)}_{p-\max}$, we can obtain the plastic radial _displacement related to the third shock wave ($u_{p3}$, Figure 8) as follows

$$u_{p3} = \frac{H3}{P_y} = 1.226 \text{ mm } (1.123 \text{ mm}) \quad (17)$$

Therefore, the maximum radial displacement after the third shock wave is $u_{p1} + u_{p2} + u_{p3} + u_{ry} = 9.093$ mm (8.159 mm). The maximum ductility ratio for Case 3S is $\mu_{3S} = (u_{p1} + u_{p2} + u_{p3} + u_{ry})/u_{ry} = 4.684$ (4.203). We can observe that the quotient between ductility ratios related to Case 3S and Case 1S is $\mu_{3S}/\mu_{1S} = 1.848$ (1.863).

The proposed unit impulse approach shows to be slightly conservative and accurate in comparison to the numerical results obtained from the SDoF analysis. The amplification factor (1.85) is similar to the value derived in Figure 7. The hysteretic energy contribution associated with each pulse is a function of the peak radial velocity, $\dot{u}_{r-\max} = \omega_n \cdot u_{ry}$, which depends on the scale of the problem (e.g. the material yielding strength). Therefore, the amplification factor related to plastic resonance depends also on this scale, that is, the amplification factor can be higher or smaller than 1.85 if other conditions are studied. However, this simplified approach can be used as an upper limit of the demand of ductility ratio including the effect of the scale.

Observe that equation (4) can be also used if certain ductility performance is required by assuming plastic resonance and the pressure time-history idealized by three (or more) unit impulses. That is, we can use an equivalent impulse ($i_r*$) in equation (4) rather than the impulse that is associated with the first shock wave ($i_r$), therefore

$$i_r* = \sqrt{2 \cdot m \cdot \left(E^{(1)}_{p-\max} + E^{(2)}_{p-\max} + E^{(3)}_{p-\max}\right)} = 2.839 \text{ MPa} \cdot \text{ms} \Rightarrow \frac{i_r*}{i_r} = 1.434 \quad (18)$$

where $E^{(1)}_{p-\max}, E^{(2)}_{p-\max}$, and $E^{(3)}_{p-\max}$ depend on the chamber thickness, which also depends on these values; therefore, the problem need to be iteratively solved.

The equivalent impulse ($i_r*$) depends on the scale of the problem, and it is not equal to the sum of impulses of the three different shock waves (1.75). Observe that $i_r*/i_r$ can be higher than 1.75 under certain circumstances. The factor 1.75 is valid when the system does not show a vibratory response, that is, when the natural frequency is substantially smaller than the reverberating frequency.

If we assume that the three pulses increase the total impulse by 1.75, we obtain that $E^{(1)}_{p-\max}* = H1* = (1.75 \cdot i_r)^2/2m = 68.6$ MPa · mm, then $u_{p1}* = 11.128$ mm, $\mu_{3S}* = 6.733$, and $\mu_{3S}*/\mu_{1S} = 2.656$. This means that the amplification factor is higher than the value obtained with the unit impulse approach.

If we assume that all variables remain constant in equation (4) except the equivalent impulse, one can determinate the ductility ratio for the case of multiple shock waves in terms of the ductility ratio for Case 1S and the equivalent impulse amplification factor ($i_r*/i_r$)

$$\mu_{3S} = \left(\frac{i_r*}{i_r}\right)^2 \cdot \left(\mu_{1S} - \frac{1}{2}\right) + \frac{1}{2} \quad (19)$$

Evaluating this equation for $\mu_{1S} = 2.535$ and $i_r*/i_r = 1.434$, we can obtain $\mu_{3S} = 4.684$ and $\mu_{3S}/\mu_{1S} = 1.848$ (same results that have been obtained above). If $i_r*/i_r = 1.75$, we obtain $\mu_{3S}* = 6.733$ and $\mu_{3S}*/\mu_{1S} = 2.656$. This calculation shows that equation (4) can be used if a proper equivalent impulse

($i_r*$) is used for design. From Figure 12, we observe that the gas pressure component increases the ductility ratio demand. For this example, the maximum radial response was 8.159 mm for Case 3S ($\mu_{3S} = 4.203$), 9.353 mm for Case 3S + QSG ($\mu_{3S+QSG} = 4.819$), and 9.082 mm for Case 3S + TG ($\mu_{3S+QSG} = 4.679$). That is, $\mu_{3S+QSG}/\mu_{3S} = 1.15$ and $\mu_{3S+TG}/\mu_{3S+QSG} = 0.97$, implying that the gas pressure increases the ductility ratio on 15% and ventilation can reduce just 3% the ductility ratio. It is interesting to note that the increment of the ductility ratio due to the gas pressure is around the same order of magnitude that the increment observed when the unit impulse approach is used (an upper limit for Case 3S).

The gas pressure component causes a uniform tensile membrane stress that can be obtained from the static part of the equation of motion (equation (1)) and equal to $\sigma^{gas}(t) = a \cdot p^{gas}(t)/(2 \cdot h)$ (normal stresses) for spherical chambers, owing to the high natural frequency of the RBM. The QS gas pressure increases the average stress of the chamber wall, and so, the chance of plastic deformation. Since, $\sigma^{gas}(t)$ is a quasi-static function, it can be equivalently included during the presented analysis using a reduction of the yielding strength during each reflection according to $\sigma_y^{eff}(t) = \sigma_y - \sigma^{gas}(t)$.